Electronic Supplementary Information

Switching from ultrafast electron transfer to proton transfer in excited drug-protein complexes upon biotransformation

Lorena Tamarit, Meryem El Ouardi, Emilio Lence, Inmaculada Andreu, Concepción González-Bello, Ignacio Vayá, Miguel A. Miranda

Fig. S1 Phosphorescence spectra for GFT-MB in a solid matrix of ethanol at 77 K after excitation at 340 nm.

Fig. S2 LFP decay traces at 600 nm for solutions containing GFT (120 μM) in the presence of increasing amounts (6, 12, 18 and 24 mM) of NAc-TrpMe (A) and NAc-TyrMe (B). Measurements were performed in deaerated MeCN after excitation at 355 nm.

Fig. S3 A) LFP spectra monitored 0.08 μs after the laser pulse for GFT-MB (black) and a mixture of GFT-MB/NAc-TyrMe in a 1:200 molar ratio (blue); the concentration of GFT-MB was 120 μM. B) Kinetic trace at 400 nm. Measurements were performed in deaerated MeCN after excitation at 355 nm.

Fig. S4 Stern-Volmer plots for the quenching of the singlet excited state of A) GFT (30 μM) in the presence of increasing amounts of NAc-TyrMe (1:50, 1:80, 1:150 and 1:200), B) GFT-MB (20 μM) in the presence of increasing amounts of 3-methylindole (1:50, 1:100, 1:150, 1:200 and 1:250), and C) GFT-MB (20 μM) in the presence of increasing amounts of NAc-TyrMe (1:20, 1:50, 1:80, 1:150 and 1:200). All measurements were performed in toluene under aerated conditions at λ_{exc} = 340 nm.

Fig. S5 Normalized UV absorption spectra at different pH values (2, black; 6, red; 7.5, blue; 8, green; 10, magenta and 12, orange) for (A) GFT and (B) GFT-MB in aqueous solution.

Fig. S6 UV absorption Job plot for (A) GFT@HSA and (B) GFT-MB@HSA at a total concentration of 20 μM in PBS. Binding mode of GFT (C) and GFT-MB (D) within HSA obtained by MD simulation studies.

Fig. S7 Fluorescence spectra of ligand@protein complexes (10 μM) at λ_{exc} = 340 nm in aerated aqueous PBS for (A) GFT-MB@HSA 1:1 (black), GFT-MB@HSA+WRF 1:1:1 (red) and GFT-MB@HSA+IBP 1:1:1 (blue) and (B) GFT-MB@HSA 1:1 (black), GFT@HSA 1:1 (red), GFT-MB@HSA+GFT 1:1:1 (blue).

Fig. S8 Normalized UV absorption spectra for aqueous solutions at different pH values (6, red; 7.5, blue; 8, green and 10, magenta) for (A) GFT@HSA and (B) GFT-MB@HSA in aqueous solution.

Fig. S9 Normalized UV spectra at the maximum absorption for mixtures containing GFT/HSA (A) and GFT-MB/HSA (B) in aqueous PBS at physiological pH.

Fig. S10 Fluorescence spectra at different pH values (2, black; 6, red; 7.5, blue; 8, green; 10, magenta and 12, orange) for (A) GFT, (B), GFT-MB, (C) GFT@HSA and (D) GFT-MB@HSA. All measurements were performed at λ_{exc} = 340 nm in aerated media. Insets show a zoom of the weakly emitting species.

Fig. S11 Fluorescence decays for GFT@HSA (black line) and GFT-MB@HSA (black dashed line) after excitation at 340 nm. All mixtures were at 1:1 molar ratio in PBS under air, using isoabsorptive solutions at the excitation wavelength.

Fig. S12 LFP decay traces for GFT-MB in deaerated MeCN (black) and GFT-MB@HSA in aerated aqueous PBS solution after excitation at 355 nm.

Fig. S13 RMSD Plots for the protein backbone (Cα, C, O and N atoms, black lines) (left) and the ligands and its quinazoline core (right) calculated from the MD simulations of the complexes: (A) GFT@HSA and (B) GFT-MB@HSA. Note the low rmsd values of the protein backbone as well as the quinazoline moiety, which is the less flexible part of each ligand. Both facts reveal the high stability of the protein complexes as well as of the ligand within the binding pocket. For GFT-MB@HSA, after ~15 ns of simulation, GFT-MB moves away from the position identified by docking towards the bottom of the pocket to

establish a hydrogen bonding interaction with the main carbonyl group of Val116, remaining fixed in this arrangement during the rest of the simulation.

Fig. S14 Variation of the relative distance between the mass center of the phenol group in Tyr161 and GFT in the drug@HSA complex during the whole simulation. Note how the tyrosine side chain in Tyr161 remains located on top of the quinazoline moiety during the simulation, with average distance of 3.7 Å (considering the last 80 ns of simulation).

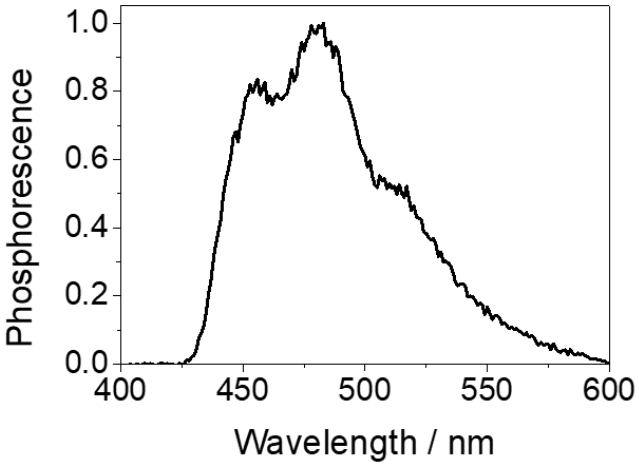

Fig. S1 Phosphorescence spectra for GFT-MB in a solid matrix of ethanol at 77 K after excitation at 340 nm.

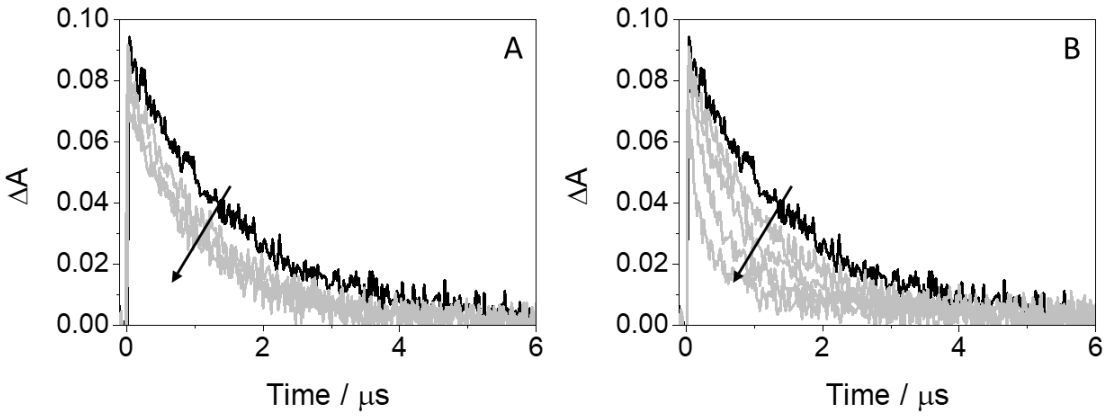

Fig. S2 LFP decay traces at 600 nm for solutions containing GFT (120 μM) in the presence of increasing amounts (6, 12, 18 and 24 mM) of NAc-TrpMe (A) and NAc-TyrMe (B). Measurements were performed in deaerated MeCN after excitation at 355 nm.

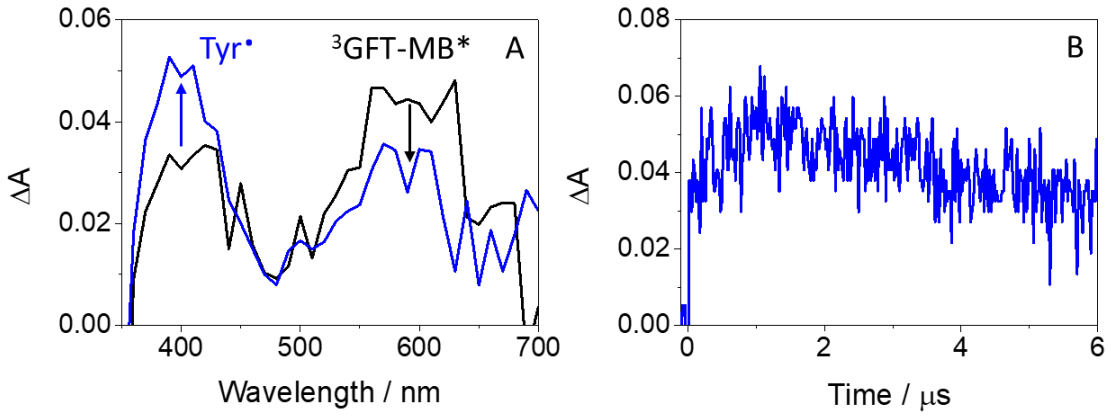

Fig. S3 A) LFP spectra monitored 0.08 μs after the laser pulse for GFT-MB (black) and a mixture of GFT-MB/NAc-TyrMe in a 1:200 molar ratio (blue); the concentration of GFT-MB was 120 μM. B) Kinetic trace at 400 nm. Measurements were performed in deaerated MeCN after excitation at 355 nm.

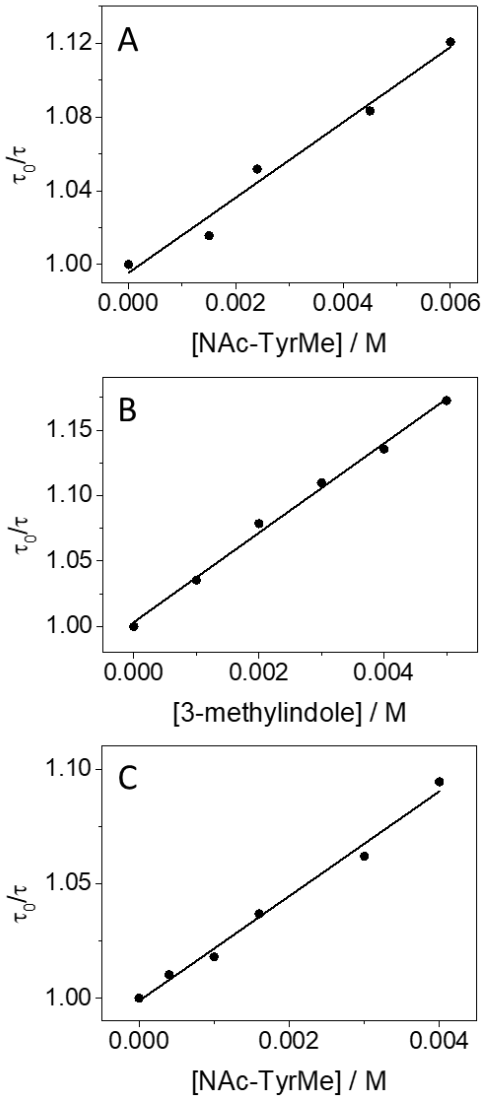

Fig. S4 Stern-Volmer plots for the quenching of the singlet excited state of A) GFT (30 μM) in the presence of increasing amounts of NAc-TyrMe (1:50, 1:80, 1:150 and 1:200), B) GFT-MB (20 μM) in the presence of increasing amounts of 3-methylindole (1:50, 1:100, 1:150, 1:200 and 1:250), and C) GFT-MB (20 μM) in the presence of increasing amounts of NAc-TyrMe (1:20, 1:50, 1:80, 1:150 and 1:200). All measurements were performed in toluene under aerated conditions at λ_{exc} = 340 nm.

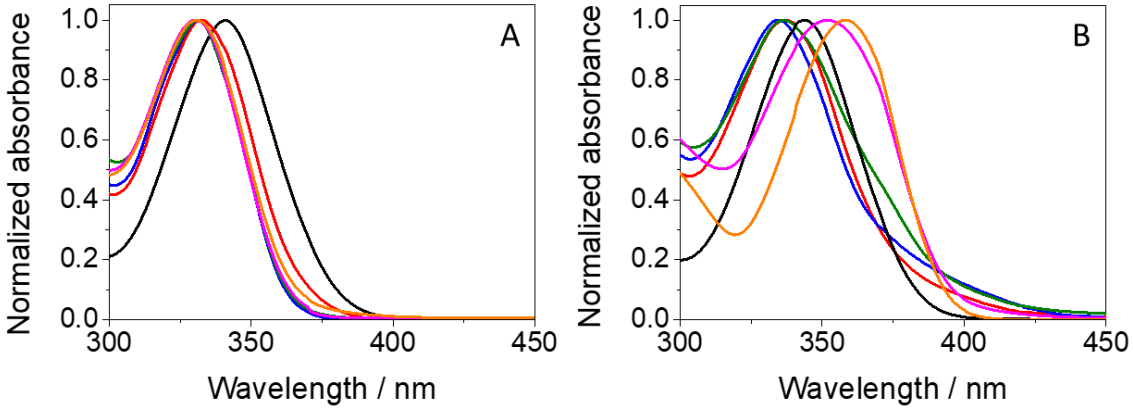

Fig. S5 Normalized UV absorption spectra at different pH values (2, black; 6, red; 7.5, blue; 8, green; 10, magenta and 12, orange) for (A) GFT and (B) GFT-MB in aqueous solution.

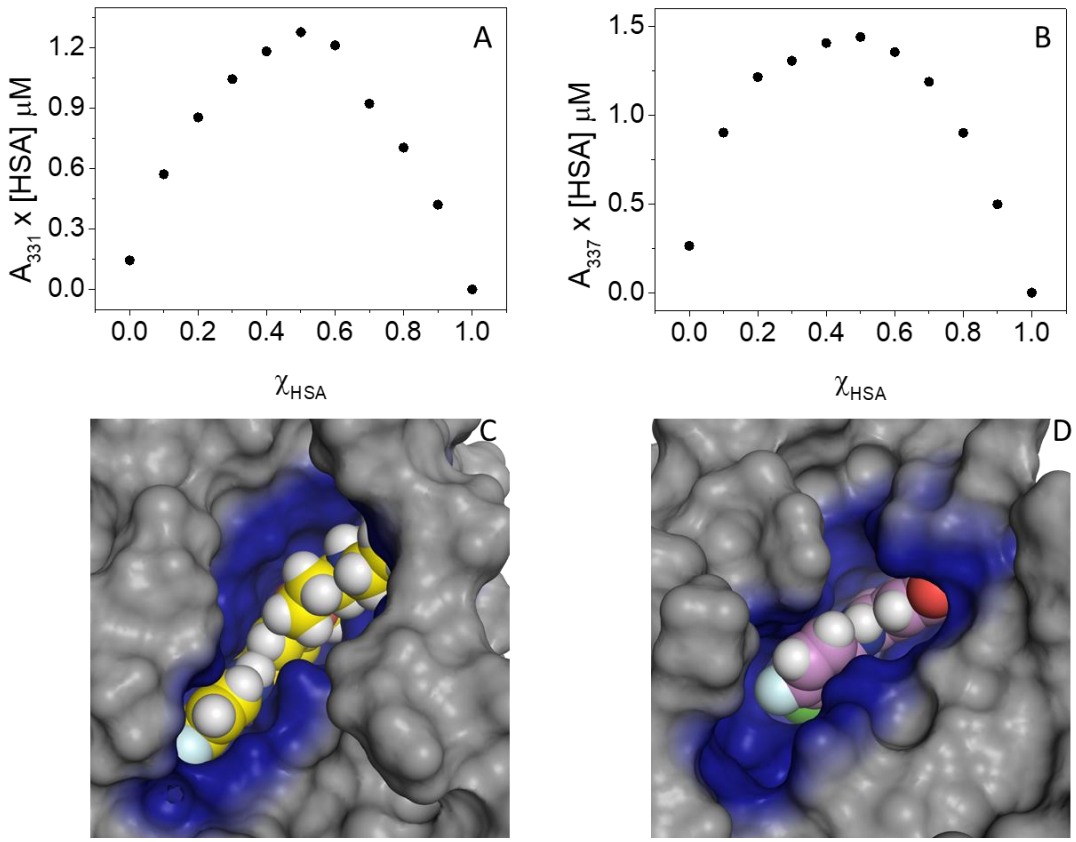

Fig. S6 UV absorption Job plot for (A) GFT@HSA and (B) GFT-MB@HSA at a total concentration of 20 μM in PBS. Binding mode of GFT (C) and GFT-MB (D) within HSA obtained by MD simulation studies.

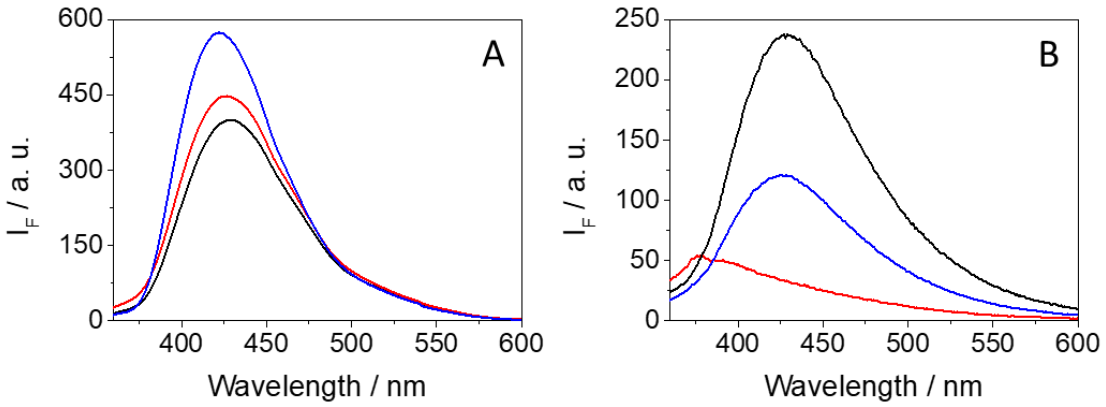

Fig. S7 Fluorescence spectra of ligand@protein complexes (10 μM) at λ_{exc} = 340 nm in aerated aqueous PBS for (A) GFT-MB@HSA 1:1 (black), GFT-MB@HSA+WRF 1:1:1 (red) and GFT-MB@HSA+IBP 1:1:1 (blue) and (B) GFT-MB@HSA 1:1 (black), GFT@HSA 1:1 (red), GFT-MB@HSA+GFT 1:1:1 (blue).

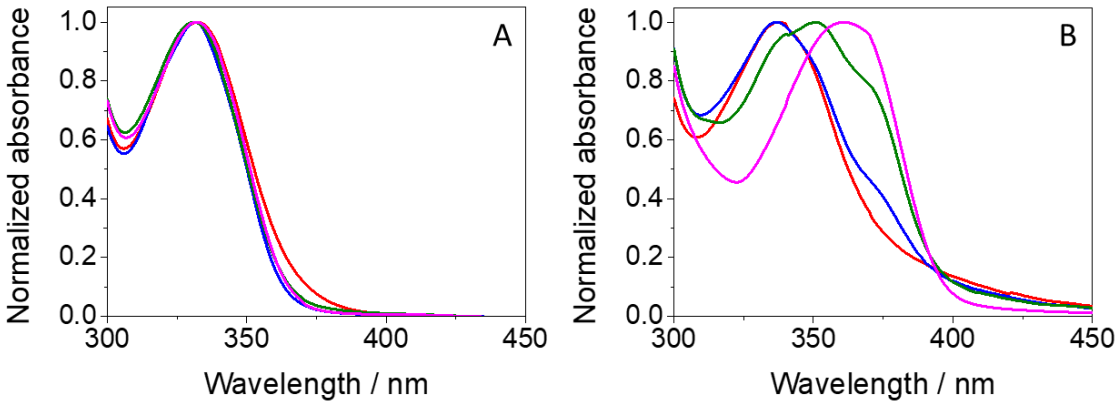

Fig. S8 Normalized UV absorption spectra for aqueous solutions at different pH values (6, red; 7.5, blue; 8, green and 10, magenta) for (A) GFT@HSA and (B) GFT-MB@HSA in aqueous solution.

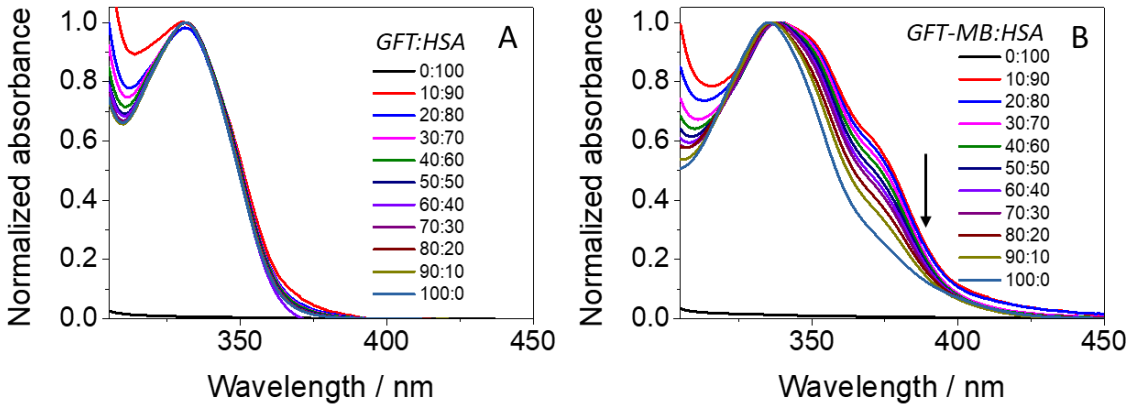

Fig. S9 Normalized UV spectra at the maximum absorption for mixtures containing GFT/HSA (A) and GFT-MB/HSA (B) in aqueous PBS at physiological pH.

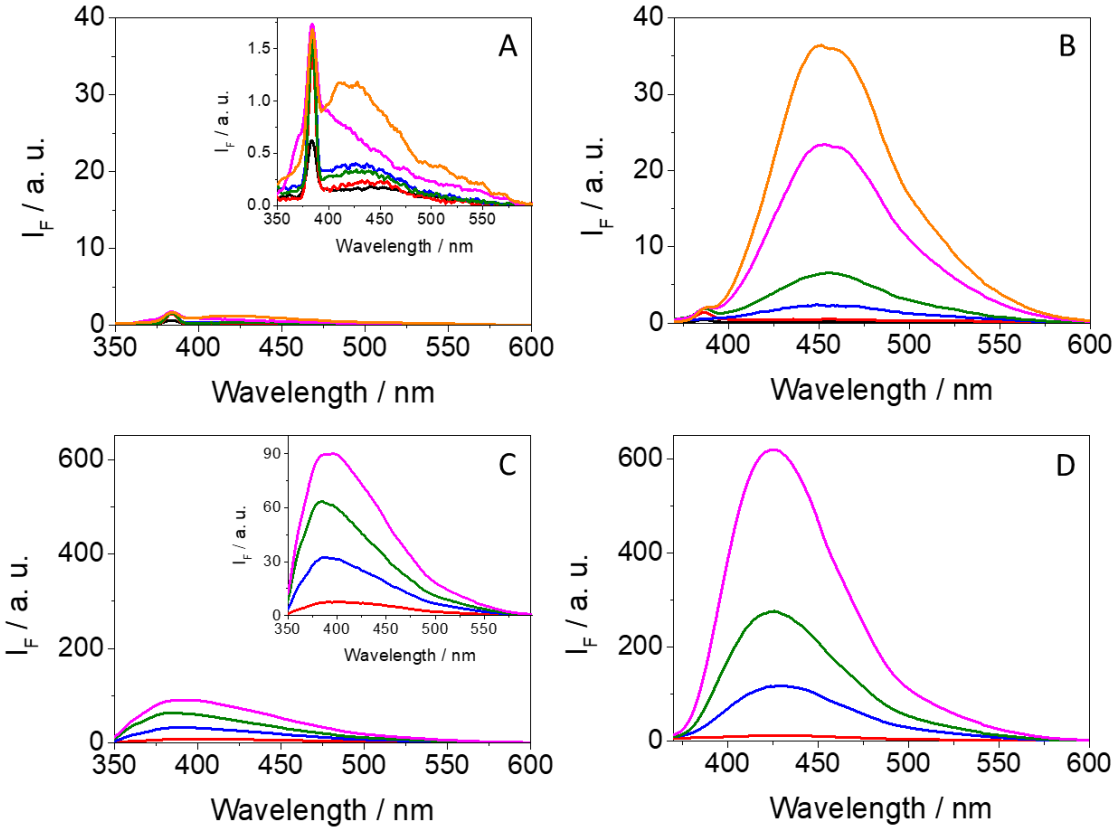

Fig. S10 Fluorescence spectra at different pH values (2, black; 6, red; 7.5, blue; 8, green; 10, magenta and 12, orange) for (A) GFT, (B), GFT-MB, (C) GFT@HSA and (D) GFT-MB@HSA. All measurements were performed at λ_{exc} = 340 nm in aerated media. Insets show a zoom of the weakly emitting species.

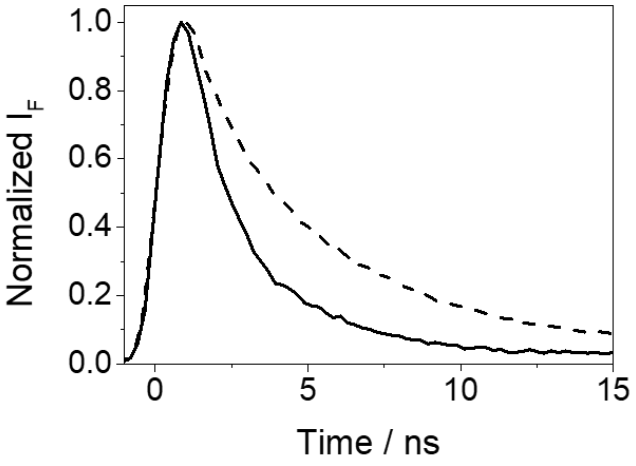

Fig. S11 Fluorescence decays for GFT@HSA (black line) and GFT-MB@HSA (black dashed line) after excitation at 340 nm. All mixtures were at 1:1 molar ratio in PBS under air, using isoabsorptive solutions at the excitation wavelength.

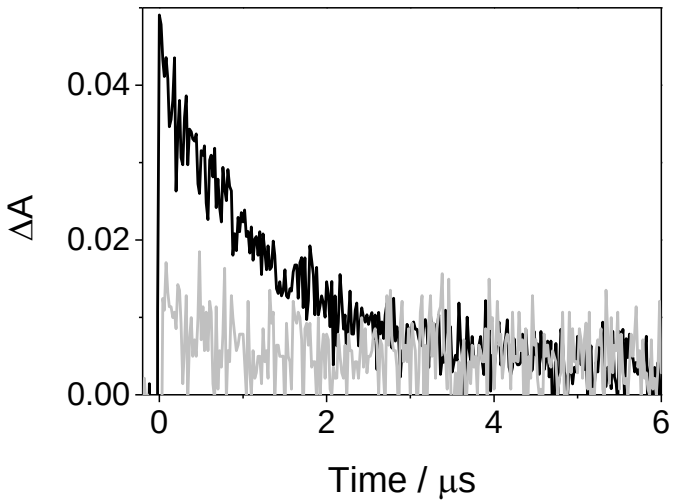

Fig. S12 LFP decay traces for GFT-MB in deaerated MeCN (black) and GFT-MB@HSA in aerated aqueous PBS solution after excitation at 355 nm.

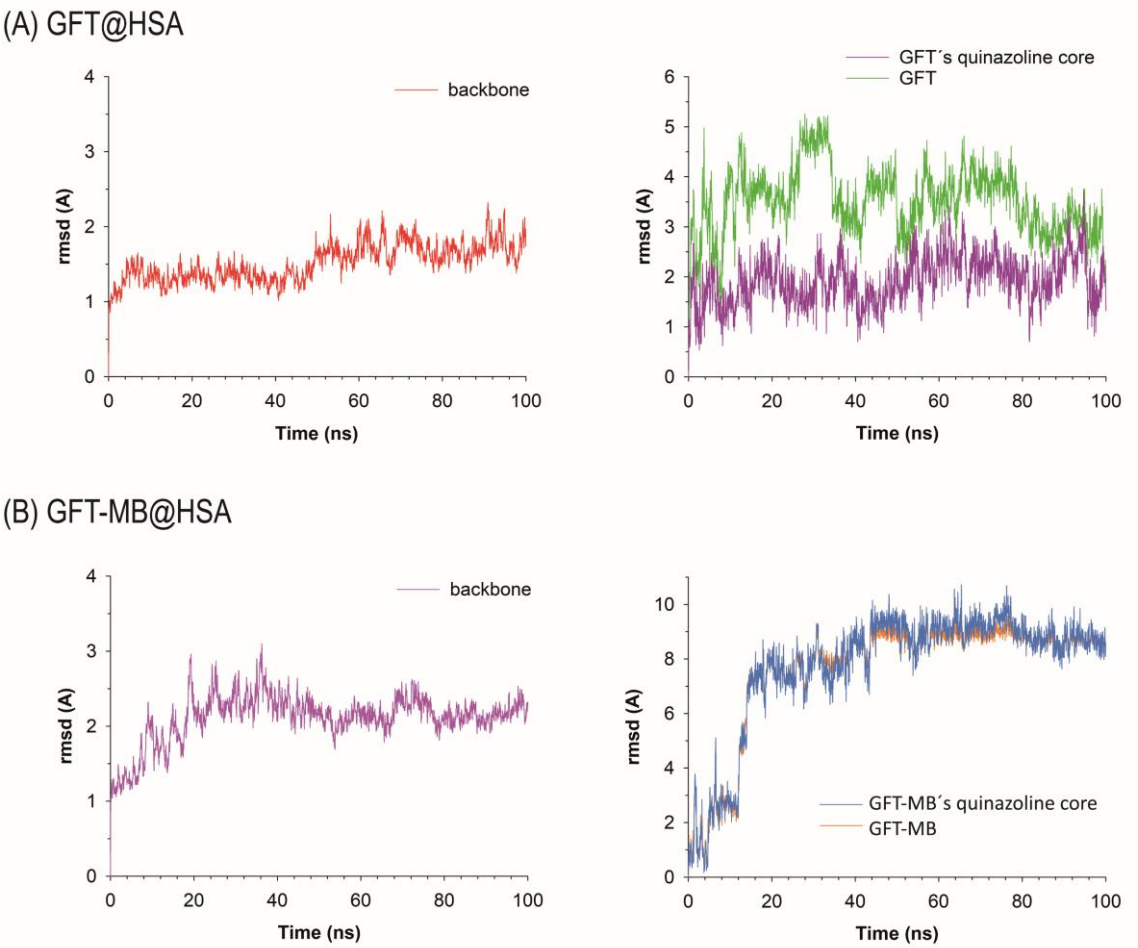

Fig. S13 RMSD Plots for the protein backbone (Cα, C, O and N atoms, black lines) (left) and the ligands and its quinazoline core (right) calculated from the MD simulations of the complexes: (A) GFT@HSA and (B) GFT-MB@HSA. Note the low rmsd values of the protein backbone as well as the quinazoline moiety, which is the less flexible part of each ligand. Both facts reveal the high stability of the protein complexes as well as of the ligand within the binding pocket. For GFT-MB@HSA, after ~15 ns of simulation, GFT-MB moves away from the position identified by docking towards the bottom of the pocket to establish a hydrogen bonding interaction with the main carbonyl group of Val116, remaining fixed in this arrangement during the rest of the simulation.

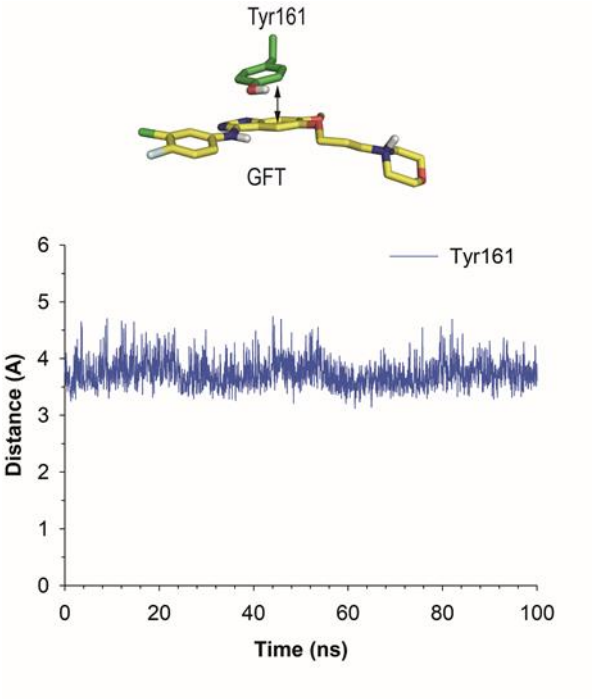

Fig. S14 Variation of the relative distance between the mass center of the phenol group in Tyr161 and GFT in the drug@HSA complex during the whole simulation. Note how the tyrosine side chain in Tyr161 remains located on top of the quinazoline moiety during the simulation, with average distance of 3.7 Å (considering the last 80 ns of simulation).